Vibro-Acoustics Modal Testing at NASA Langley Research Center

Richard S. Pappa and Jocelyn I. Pritchard
Structural Dynamics Branch
NASA Langley Research Center
Hampton, VA 23681

Ralph D. Buehrle
Structural Acoustics Branch
NASA Langley Research Center
Hampton, VA 23681

ABSTRACT

This paper summarizes on-going modal testing activities at the NASA Langley Research Center for two aircraft fuselage structures: a generic "aluminum testbed cylinder" (ATC) and a Beechcraft Starship fuselage (BSF). Subsequent acoustic tests will measure the interior noise field created by exterior mechanical and acoustic sources. These test results will provide validation databases for interior noise prediction codes on realistic aircraft fuselage structures. The ATC is a 12-ft-long, all-aluminum, scale model assembly. The BSF is a 40-ft-long, all-composite, complete aircraft fuselage. To date, two of seven test configurations of the ATC and all three test configurations of the BSF have been completed. The paper briefly describes the various test configurations, testing procedure, and typical results for frequencies up to 250 Hz.

INTRODUCTION

Aircraft interior noise reduction is a multidisciplinary problem involving both structural and acoustic aspects (Ref. 1). Current research focuses on developing validated analytical models of sound transmission through complex structures and within vehicle interiors, forming the basis of design tools for interior noise prediction and control. The work discussed in this paper is one aspect of a collaborative effort in this area between the Structural Dynamics Branch (Ref. 2) and the Structural Acoustics Branch (Ref. 3) at NASA Langley Research Center.

Two fuselage structures are being used for validation of various interior noise prediction codes (such as NASTRAN, COMET/Acoustics, and Boeing's Matrix Difference Equation technique). The first structure is an in-house-designed, generic "aluminum testbed cylinder" (ATC). The ATC is an all-aluminum, ring-and-stringer stiffened cylinder 12 ft in length and 4 ft in diameter that uses representative aircraft construction. It consists of a cylindrical shell, floor, and end cap components, allowing testing to occur at various stages of assembly. Final phases in the program will use a pressurized interior of up to 7 psi to simulate flight conditions.

The second structure is a complete Beechcraft Starship fuselage (BSF), manufactured about 10 years ago during the development phase of the commercial vehicle. The BSF is an all-composite, reinforced shell 40 ft in length and 6 ft in diameter (in the cabin section) constructed using honeycomb core and graphite-epoxy face sheets. Figure 1 shows the Beechcraft Starship in operation. The Starship is a 10-passenger business aircraft with aft-mounted pusher turboprops, variable-sweep canards, and large winglets that serve as vertical stabilizers. It was the first all-composite plane certified by the FAA. Approximately 50 Starships are currently in service.

This paper summarizes on-going modal tests of the ATC and BSF being conducted for validation of structural finite-element models. Subsequent acoustic tests will measure the interior noise field created by exterior mechanical and acoustic sources. The test objective is to identify the modal parameters (natural vibration frequencies, damping, and mode shapes) of each testbed configuration to as high a frequency as possible. References 4 and 5 contain supplemental information on the structural modeling and model updating aspects of the project. This paper covers only the modal testing activities.

TEST CONFIGURATIONS

Table 1 lists the seven test configurations of the ATC and the three test configurations of the BSF. To date, the first two tests in the ATC program and all three tests in the BSF program have been completed. Figure 2 shows both structures in their initial modal test configurations. The first ATC test article consisted of the bare ring-and-stringer frame. The first BSF test article consisted of the bare fuselage without side windows or door. Each structure was mounted on soft supports to simulate free-free boundary conditions. The ATC used bungee cord at each end, and the heavier Starship fuselage used four air bags. Figure 3 shows a close-up view of the two rear airbags supporting the BSF. Two additional units supported the front of the vehicle. Test configurations 4 through 7 of the ATC will switch over to a similar airbag support system because of the increased weight of these assemblies.

Figure 4 shows ATC configurations 2 and 3. Configuration 2 adds two 100-lb particleboard end plates to the framework. The end plates provide stiff, terminating reflective surfaces for the enclosed acoustic cavity. They contain several ½-in-diameter holes designed to allow the pressure on both sides of the end plates to equalize during pressurized tests. Configuration 3 adds a 0.040-in-thick aluminum skin. The skin is attached along each of the 11 equally spaced ring frames and the 24 equally spaced stringers with a double line of rivets and epoxy. This attachment assures airtight operation at internal pressures up to 7 psi. Figure 5(a) shows the end domes for the ATC. They are ¼-inch-thick fiberglass composite structure weighing approximately 80 lb each. The end domes are designed to safely carry the interior pressure loads without applying a bending load to the cylinder. The ATC floor, shown in Fig. 5(b), uses dense-core aluminum honeycomb construction. It is supported by a row of stiff aluminum cross members spanning each ring frame. The floor lies 9 inches below the centerline of the cylinder. Fully assembled, the aluminum testbed cylinder weighs approximately 600 lb.

Figure 6 shows interior views of the Starship fuselage. The interior space is essentially empty except for the seat rails and a few miscellaneous items on or near the firewall and in the nose of the aircraft. All of the side window openings are identical in size except for the second-last one on the right side of the plane, visible in the upper-left corner of Fig. 6(b). This larger window is an emergency exit for passengers. Fully assembled (with side windows and door), the BSF weighs approximately 1600 lb.

TESTING PROCEDURE

The intent of this testing is to provide a validated structural acoustic model to as high a frequency as finite-element modeling technology permits. The important motion of the structure for interior noise prediction is the normal motion of the fuselage wall, which is the only structural component that couples to the interior acoustics.

Figure 7 shows the distribution of accelerometers used in the modal tests conducted to date. These measurement positions were selected based on pre-test predictions of the first 100 modes of each structure. The 207 locations in Fig. 7(a) apply to ATC test configurations 1 through 5. ATC test configurations 6 and 7 will use approximately 50 additional accelerometers on the floor and floor supports. The 245 locations in Fig. 7(b) apply to all 3 of the BSF test configurations. Both test articles used a similar sensor distribution. Several rings around each structure were heavily instrumented with radial accelerometers primarily to characterize the "breathing" shell modes (also known as "radial-axial" modes). Several longitudinal lines were heavily instrumented with radial and biaxial accelerometers primarily to characterize the bending and torsional modes. A few triaxial accelerometers captured the secondary axial motion. The ATC sensor distribution had 5 instrumented rings and 3 instrumented longitudinal lines, and the BSF sensor distribution had 8 instrumented rings and 4 instrumented longitudinal lines. The Starship fuselage required more measurements than the aluminum cylinder because of its larger size, and also because of the structural nonuniformity caused by the holes for the side windows and door, and by the tapering of the nose and tail sections.

Figure 8 shows the shaker locations used in the modal tests. These excitation positions were also selected based on pre-test predictions of the first 100 modes of each structure. Figure 8(a) shows the four ATC shaker locations. Shaker 1 applies a tangential side force at a 45-degree angle below the horizontal direction, which primarily excites the torsional and axial modes of the structure. Shakers 2 through 4 apply radial forces at various locations, which primarily excite the bending and breathing modes of the structure. Figure 8(b) shows the seven BSF shaker locations. Shakers 1-2 and 3-4 apply lateral forces at slightly different orientation angles to the passenger cabin on its left and right sides, respectively. Shaker 5 applies a radial force to the top of the fuselage near the door position. Shakers 6 and 7 apply forces at the front wingbox attachment bolts on the left and right sides of the vehicle, respectively. All seven BSF shakers excite both the bending and breathing modes of the structure to some degree. In most ATC and BSF tests, all shakers operated simultaneously using uncorrelated, burst random or pure random excitation forces. A mechanical impedance sensor measured the input force and corresponding drive-point acceleration at each shaker location.

Figures 9 and 10 are flowcharts of the principal data-acquisition and data-analysis steps, respectively. In each modal test, all of the excitation forces and corresponding response accelerations were recorded simultaneously on a large 432-channel data acquisition system. This system has matched anti-aliasing filters, 16-bit analog-to-digital converters (ADCs), and auto-ranging capability to assure high quality measurements. Prior to digitization, the measurement chain used computer-controlled signal conditioning to optimize voltage amplitudes and low-pass (LP) noise filters on every channel to reject out-of-band instrumentation noise. The force and acceleration time histories were recorded onto several ADC throughput disks located within the data acquisition system. After each test, the time histories were transcribed (i.e., sorted by channel number) onto the system disk of the host workstation. All time histories measured in every test were also written on CD-ROMs for permanent archival data storage, allowing future reanalysis if necessary.

Next (see Fig. 10), the system disk of the host workstation was cross-mounted to a faster computer containing a suite of Fortran data analysis software. Cross-mounting the disk simply means that this software could directly read the data files located on the host workstation. The first data analysis step created high-resolution frequency response functions (FRFs) and multiple coherence functions (MCFs) using traditional multiple-input calculation techniques (Ref. 6). MCFs are commonly computed

functions that measure the reliability of the corresponding FRFs at each frequency line. Because of the large number of modes excited in each test and the relatively low damping levels of the structures, particularly the ATC, Fourier transform blocksizes as high as 64K (65,536) were used. Mode indicator functions (MIFs) were then calculated from the FRF data (Ref. 7). MIFs provide excellent estimates of the natural vibration frequencies of the structure, particularly at lower frequencies. These natural frequency estimates should correlate closely with those obtained in the rigorous modal identification step, performed next using the Eigensystem Realization Algorithm (ERA).

ERA is a multiple-input, multiple-output, time-domain technique that uses all available frequency response functions simultaneously to identify structural modal parameters. The method was developed at NASA Langley in 1984, and an accompanying Fortran software package has been continuously improved since then in conjunction with many applications. A large bibliography of ERA-related technical publications is available on the Internet (Ref. 8). The reader should consult this on-line listing for additional information on the technique.

The final data analysis step is a mode-condensation procedure that sifts through large amounts of ERA results and extracts the best, unique set of modal parameters. This recently developed technique uses an autonomous supervisor to condense multiple estimates of modal parameters using the Consistent-Mode Indicator (CMI), the principal accuracy indicator of ERA, and correlation of mode shapes (Refs. 9,10).

TYPICAL RESULTS

Experimental results are presented for the initial test configuration of each structure. Figures 11 and 12 show FRFs and MIFs in the frequency range of 0 to 250 Hz. Other data (not shown) extend to a maximum frequency of 1000 Hz. These frequency-response and mode-indicator functions show the quality and complexity of the measurements and reveal an appreciable difference between the two test articles. Specifically, the ATC frame is a lightly damped structure with corresponding lightly coupled modes, whereas the BSF is a more heavily damped structure with corresponding higher modal coupling. Higher damping and modal coupling complicate experimental modal identification. Linearity test data (not shown) also disclose a higher nonlinearity for the BSF than for the ATC frame. Nonlinearity also complicates experimental modal identification, which assumes that the structural dynamic characteristics are approximately linear (i.e., the vibration response varies linearly with the excitation force level).

Figure 11 shows only one FRF from each test, while the MIF data in Fig. 12 incorporate all of the FRFs measured in each test. Multiplying the number of accelerometers by the number of shakers, a total of 828 FRFs were obtained in the ATC modal test and a total of 1715 FRFs were obtained in the BSF modal test. The MIFs are derived from the complete set of FRFs by solving an Nth-order eigenvalue problem at each frequency line, where N is the number of shakers. To a significant degree, the dips in the MIF plots (particularly the dips that extend down to approximately zero) indicate reliably and precisely the natural frequencies of the modes of vibration. However, they provide no corresponding damping or mode shape information. Also, there is a fair amount of uncertainty concerning the number of modes in those frequency intervals with overlapping and/or shallow dips. The estimated natural frequencies from the MIF plots are not used directly in the ERA modal identification process. They are only used to correlate with and corroborate the ERA results. ERA

calculates all modal parameters (natural frequencies, damping, and mode shapes) using all FRFs simultaneously.

Approximately 100 modes of the ATC and 40 modes of the BSF have been identified below 250 Hz for each initial test configuration. Figures 13 and 14 show four typical results for each structure, arranged in order of increasing frequency. For interior noise prediction, the radial-axial modes ("breathing" modes) tend to be the most important type of modes. However, the other modes also provide valuable additional information for validating and refining the physical properties of the finite-element models, resulting in improved prediction accuracy for the acoustically important modes as well.

The radial-axial modes (Figs. 13d, 14b, and 14d) are described by parameters i and j, where i is the number of circumferential waves in the mode shape and j is the number of axial (longitudinal) half-waves in the mode shape. These modes occur in pairs at approximately the same frequency because of the circular cross-sectional shape of the fuselages. The bending modes (Figs. 13a and 14c) also occur in pairs, whereas the torsional modes (Fig. 13c) occur individually. The 1st shear mode of the ATC (Fig. 13b) has longitudinal shearing of the top of the cylinder relative to its bottom, indicated by the two end rings moving in this manner. Recall from Fig. 7 that axial accelerometers are located only on the end rings of the cylinder, so that the measured shape of the shearing modes must be carefully interpreted considering the locations and directions of the sensors. The pitch mode of the BSF (Fig. 14a) is one of six rigid-body modes of each test article. Experimentally obtained rigid-body modes are useful for validating the proper placement and functioning of the instrumentation. For example, it is not uncommon in modal tests to accidentally switch the polarity of one or more accelerometers. This error is quickly disclosed in the rigid-body modes because of their familiar shapes.

CONCLUSIONS

This paper gave a brief overview of a series of modal tests underway at NASA Langley Research Center for validation of finite-element models of two structures: 1) a generic, scale-model fuselage section known as the "aluminum testbed cylinder" (ATC) and 2) a complete Beechcraft Starship fuselage (BSF). Both test articles will be used for evaluating interior noise prediction codes. The ATC has seven distinct test configurations and the BSF has three distinct test configurations. The modal test objective for each configuration is to identify the natural vibration frequencies, damping, and mode shapes to as high a frequency as possible. To date, approximately 100 modes of the ATC and 40 modes of the BSF have been obtained below 250 Hz using the Eigensystem Realization Algorithm. The modes of the BSF are generally more difficult to identify at higher frequencies than those of the ATC due to its higher damping and modal coupling. Most of the mode shapes of both fuselage structures have a complex, three-dimensional nature, requiring many accelerometers and shakers to characterize properly.

REFERENCES

1. Ohayon, R. and Soize, C., *Structural Acoustics and Vibration*, Academic Press, San Diego, 1998.

2. Adelman, H. M., "Structural Dynamics Branch," NASA Langley Research Center, Website: http://sdb-www.larc.nasa.gov/SDBranch, August 1997.

3. Shepherd, K. P., "Structural Acoustics Branch," NASA Langley Research Center, Website: http://fmad-www.larc.nasa.gov/fmad/sab/SAB.html, February 1999.

4. Grosveld, F. W., "Structural Normal Mode Analysis of the Aluminum Testbed Cylinder (ATC)," AIAA Paper 98-1949, *Proceedings of the 39th AIAA/ASME/ASCE Structures, Structural Dynamics, and Materials Conference*, Long Beach, CA, April 1998.

5. Hassiotis, S., "Update of the Starship Fuselage Finite Element Model Using Modal Data," *Proceedings of the 17th International Modal Analysis Conference*, Kissimmee, FL, February 1999, pp. 1563-1569.

6. Allemang, R. J. and Brown, D. L., "Experimental Modal Analysis," Chapter 16 in *Handbook on Experimental Mechanics*, Prentice-Hall, Inc., Englewood Cliffs, NJ, 1987.

7. Williams, R., Crowley, J., and Vold, H., "The Multivariate Mode Indicator Function in Modal Analysis," *Proceedings of the 3rd International Modal Analysis Conference*, Orlando, FL, January 1985, pp. 66-70.

8. Pappa, R. S., "ERA Bibliography," Website: http://sdb-www.larc.nasa.gov/SDB/Research/data/ERA_biblio.html, September 1998.

9. Pappa, R. S., Elliott, K. B., and Schenk, A., "Consistent-Mode Indicator for the Eigensystem Realization Algorithm," *Journal of Guidance, Control, and Dynamics*, Vol. 16, No. 5, September-October 1993, pp. 852-858.

10. Pappa, R. S., James, G. H. III, and Zimmerman, D. C., "Autonomous Modal Identification of the Space Shuttle Tail Rudder," *Journal of Spacecraft and Rockets*, Vol. 35, No. 2, March-April 1998, pp. 163-169.

Table 1 – Modal Test Configurations

(a) Aluminum Testbed Cylinder (ATC)		
No.	**Description**	**Status**
1	Bare Frame	Completed
2	No. 1 + End Plates	Completed
3	No. 1 + Skin	In Progress
4	No. 3 + End Plates	Future
5	No. 4 + End Domes	Future
6	No. 5 + Floor (Fully Assembled)	Future
7	No. 6 + Internal Pressure	Future

(b) Beechcraft Starship Fuselage (BSF)		
No.	**Description**	**Status**
1	Bare Fuselage Without Side Windows or Door	Completed
2	No. 1 + Side Windows	Completed
3	No. 2 + Door	Completed

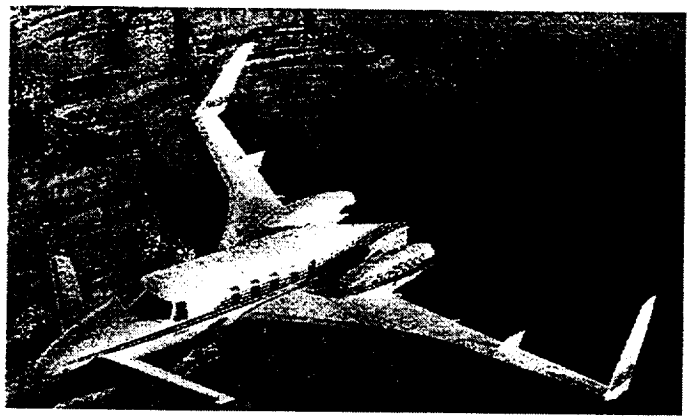

Fig. 1 – Starship in Flight

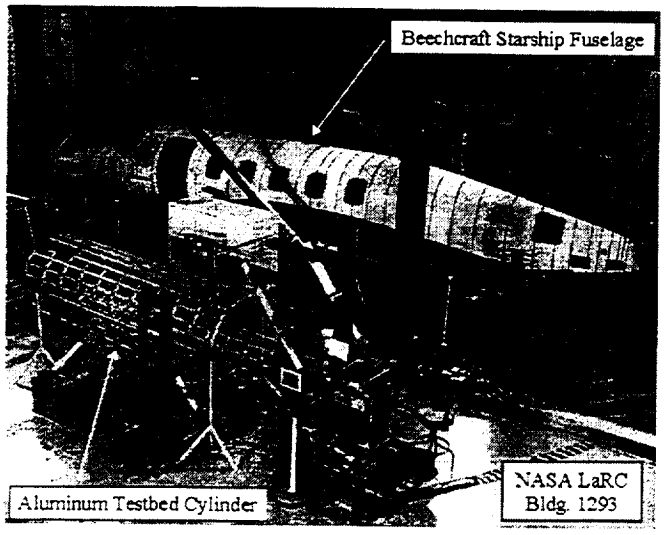

Fig. 2 – Initial Test Configurations of the ATC and BSF

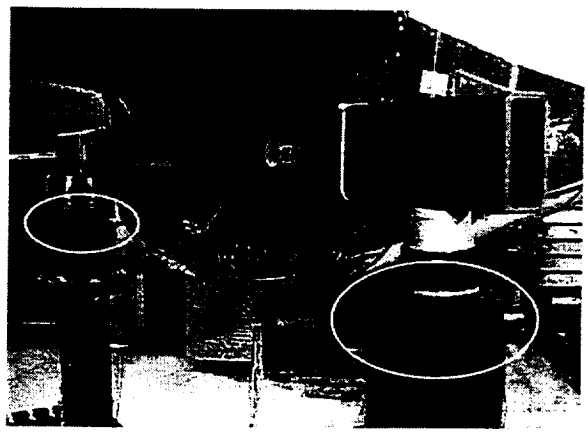

Fig. 3 – Rear BSF Airbags

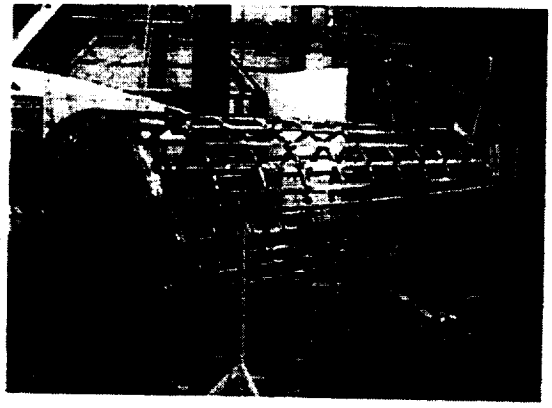

(a) Config. 2: Bare Frame + End Plates

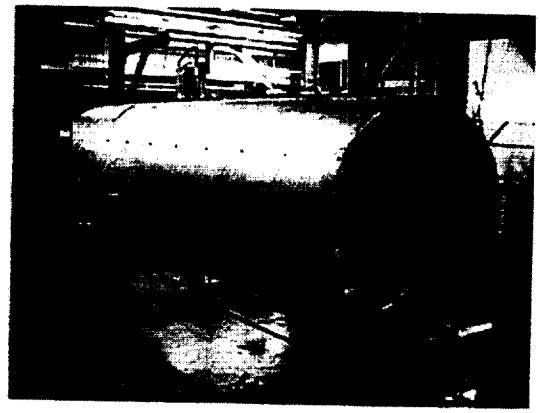

(b) Config. 3: Bare Frame + Skin

Fig. 4 – Second and Third Test Configurations of the ATC

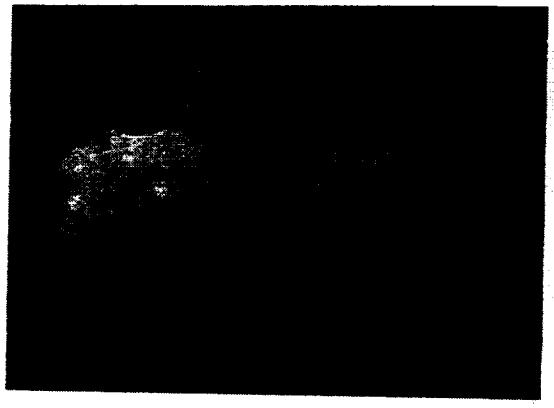

(a) End Domes

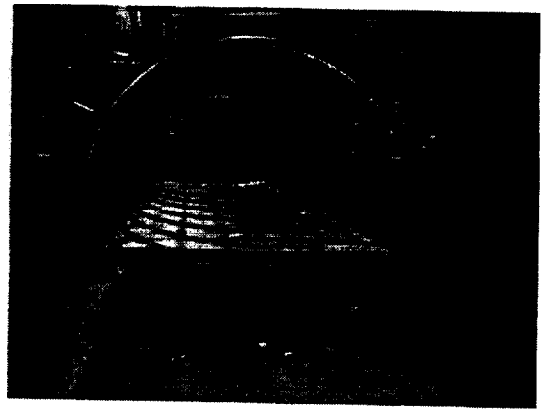

(b) Floor

Fig. 5 – Additional ATC Components

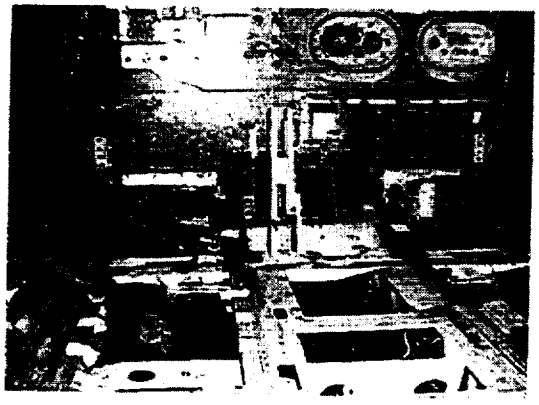

(a) Looking Forward

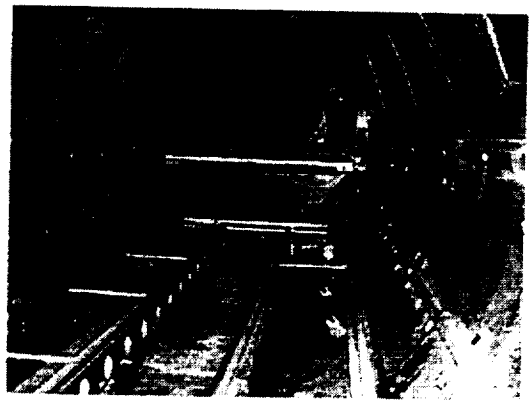

(b) Looking Aft

Fig. 6 – Interior of the BSF

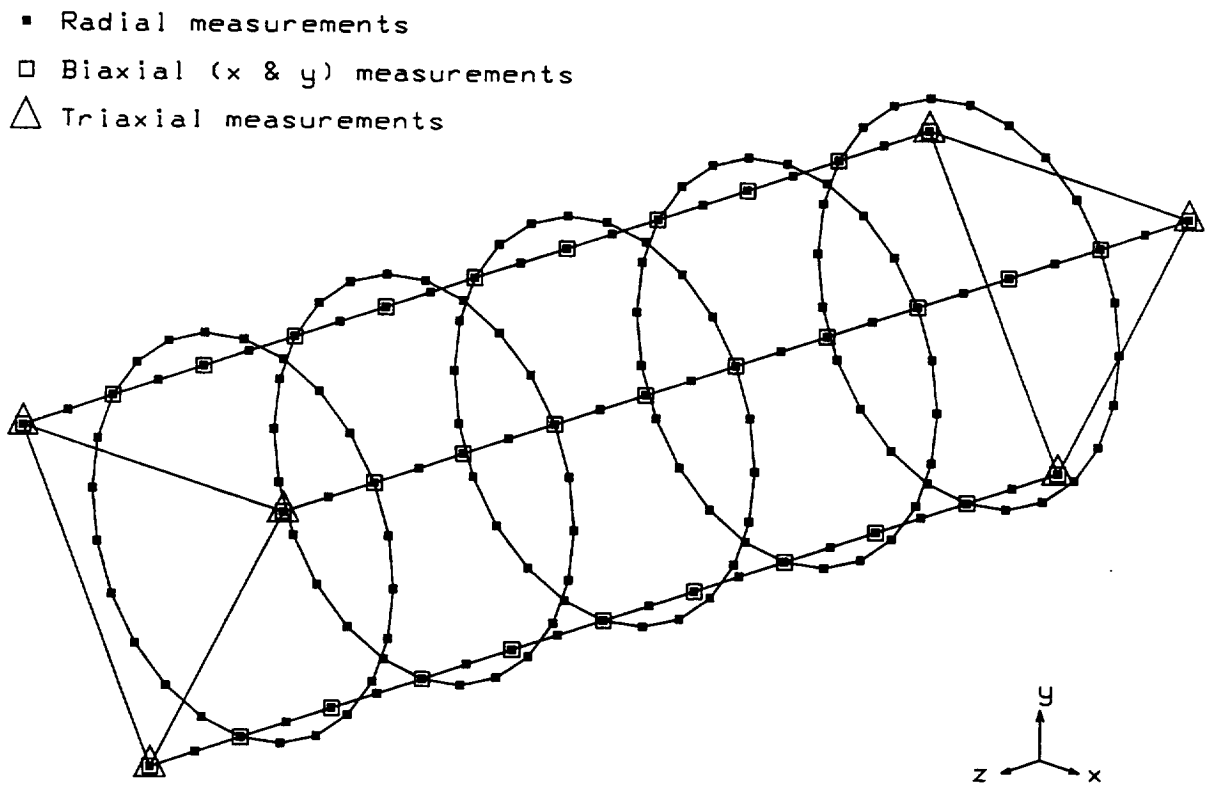

(a) 207 Accelerometers on ATC

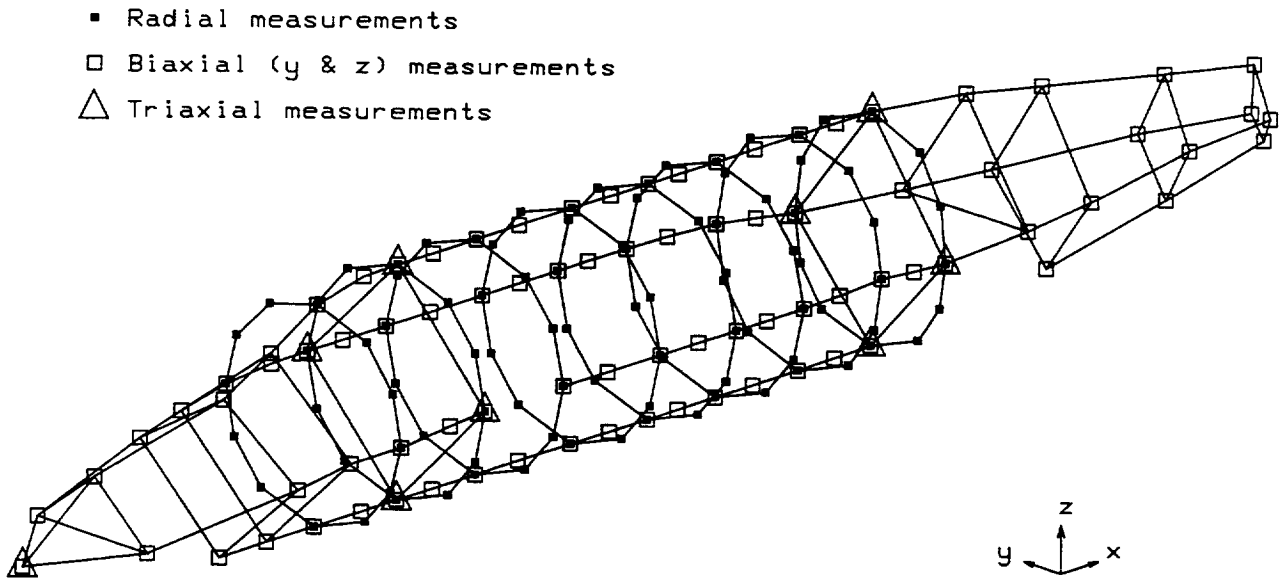

(b) 245 Accelerometers on BSF

Fig. 7 – Accelerometer Locations

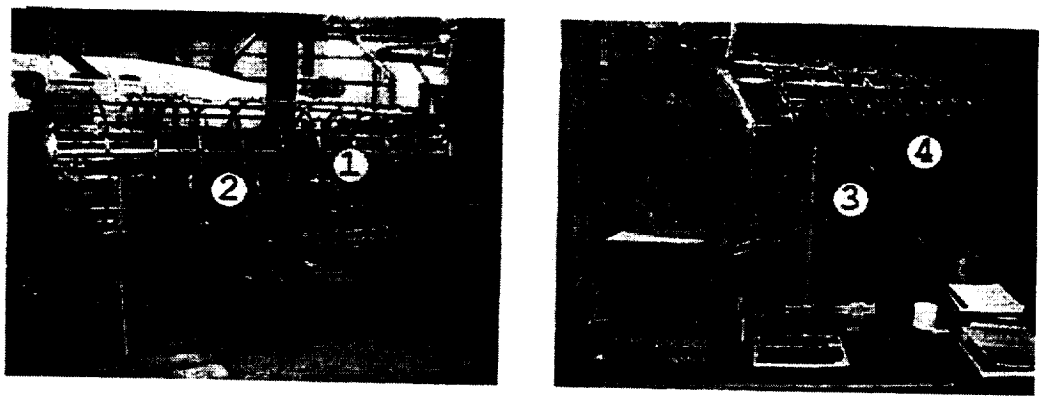

(a) 4 Shakers on ATC

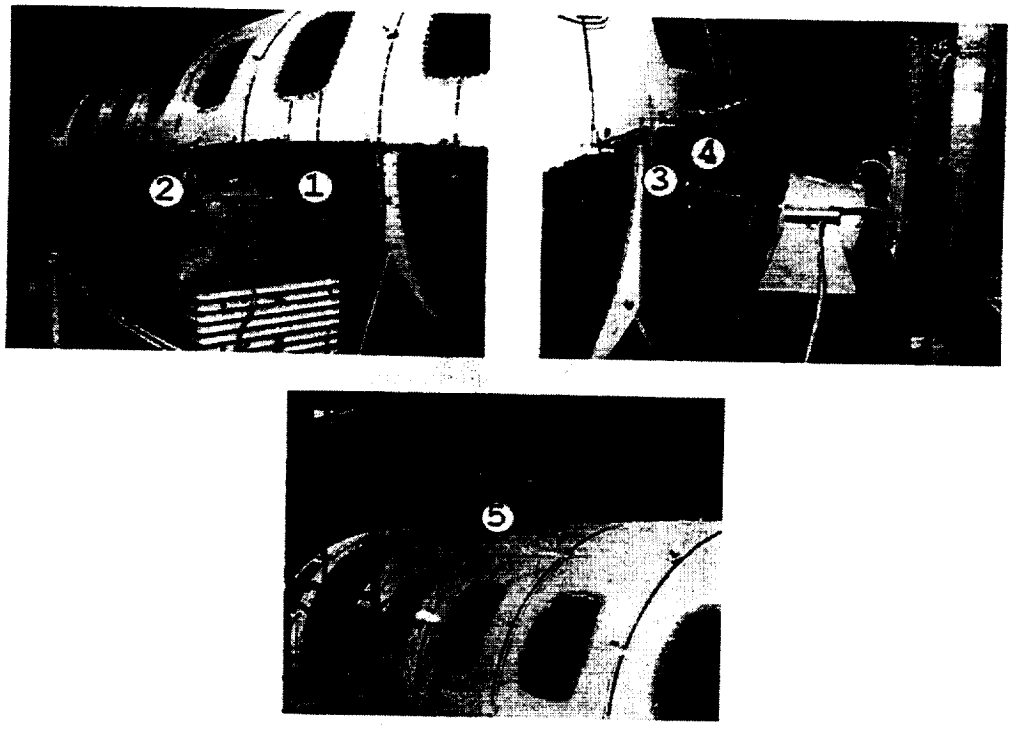

(b) 7 Shakers on BSF

Fig. 8 – Shaker Locations

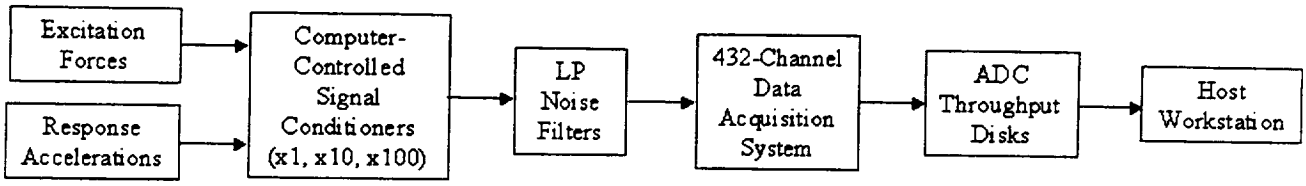

Fig. 9 – Data Acquisition Flowchart

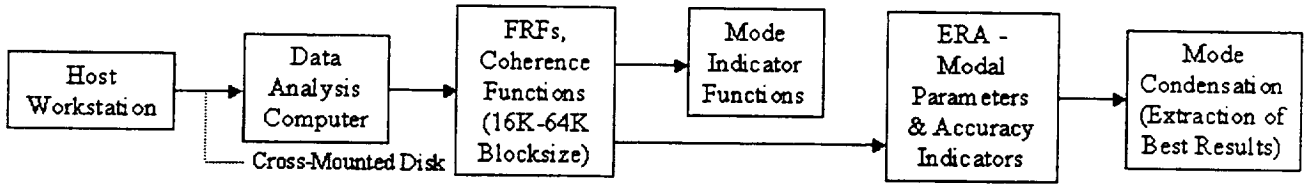

Fig. 10 – Data Analysis Flowchart

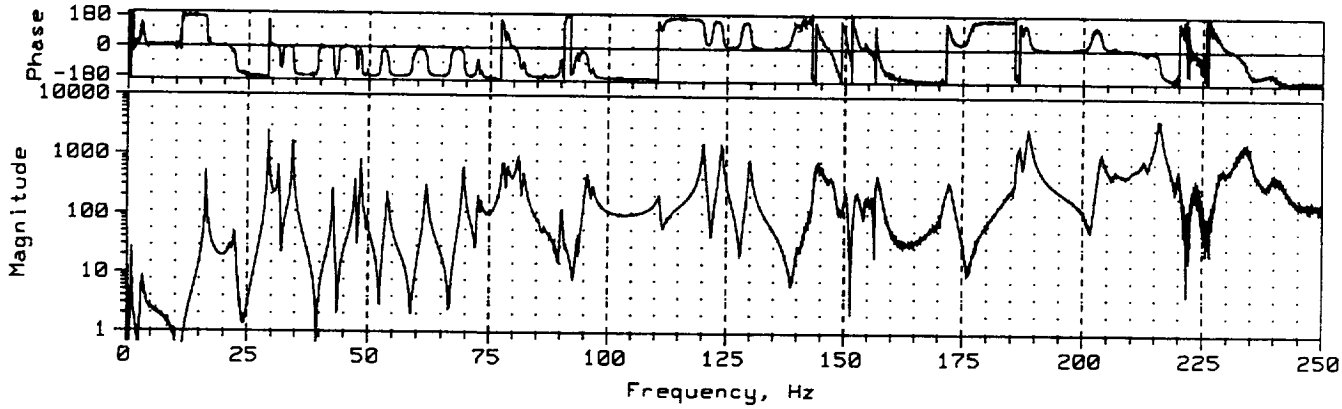

(a) ATC - Config. 1: Bare Frame

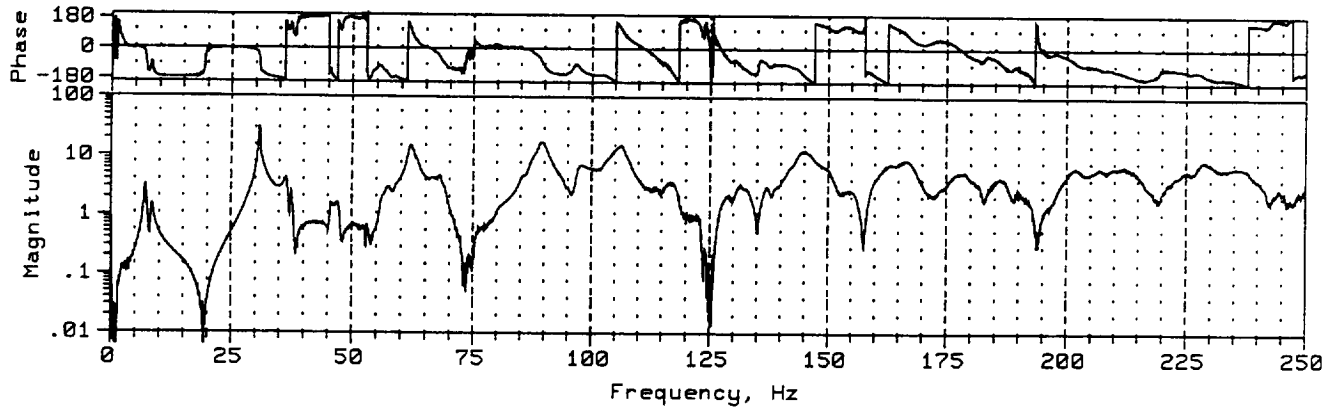

(b) BSF - Config. 1: Bare Fuselage Without Side Windows or Door

Fig. 11 – Typical Frequency Response Functions

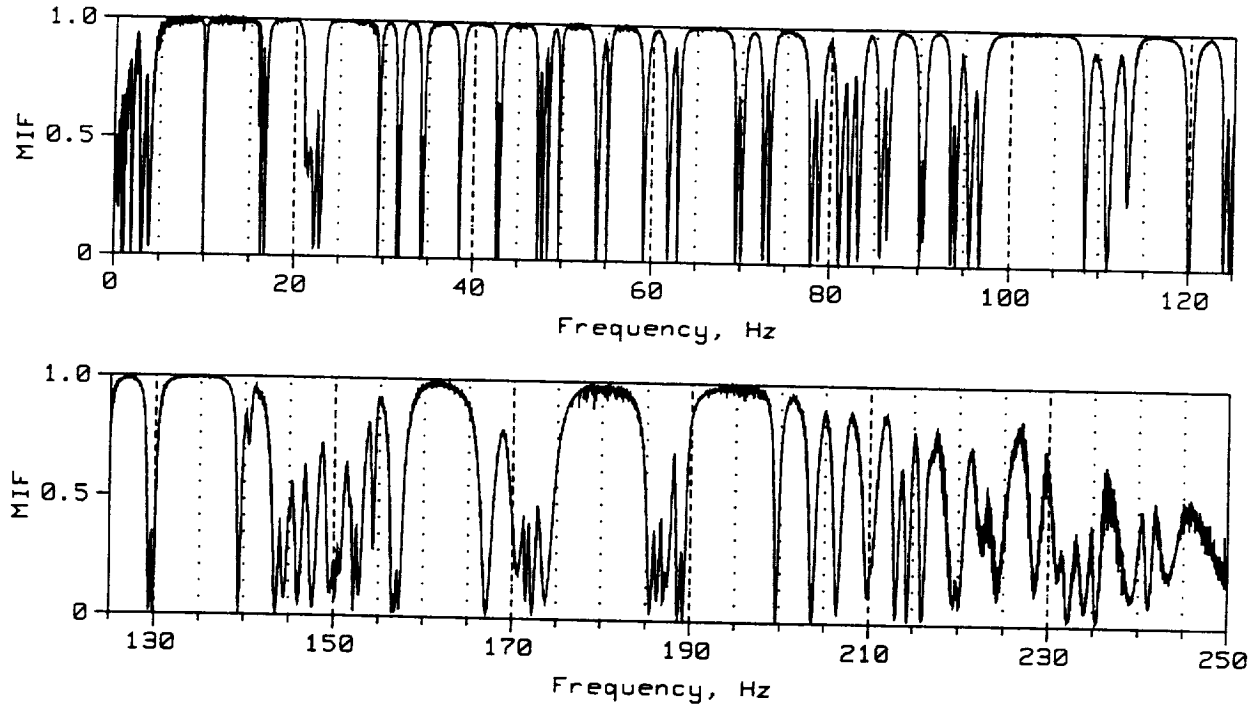

(a) ATC - Config. 1: Bare Frame

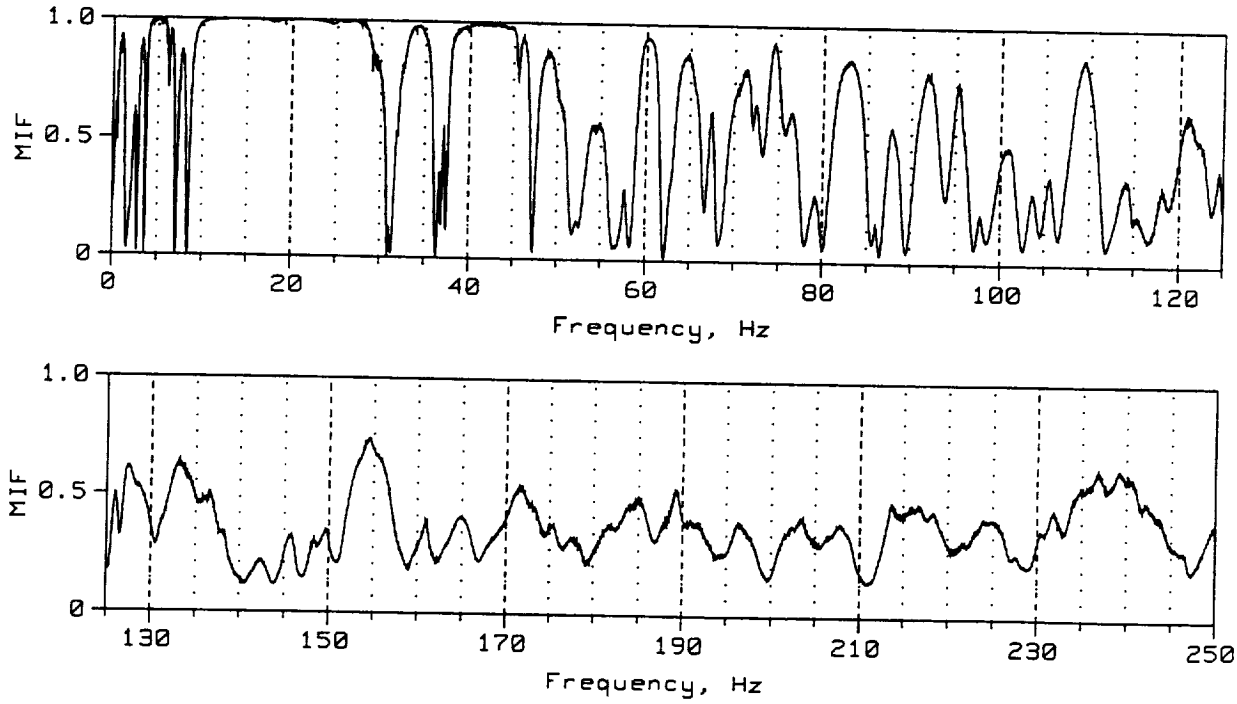

(b) BSF - Config. 1: Bare Fuselage Without Side Windows or Door

Fig. 12 – Mode Indicator Functions (Dips Indicate Natural Frequencies)

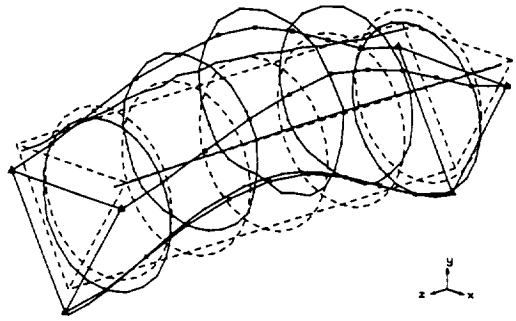

(a) 1st Vertical Bending Mode (16.7 Hz)

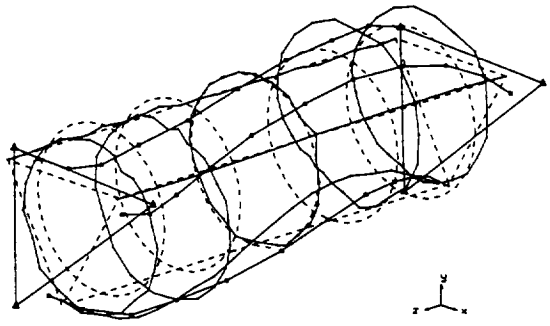

(b) 1st Shear Mode (22.5 Hz)

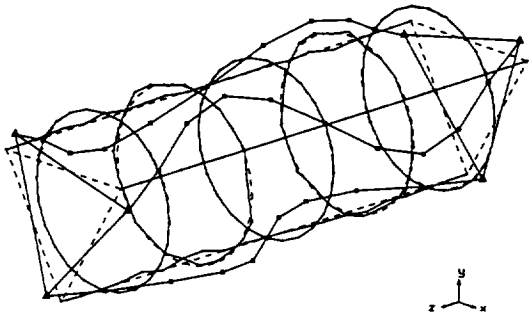

(c) 3rd Torsion Mode (38.5 Hz)

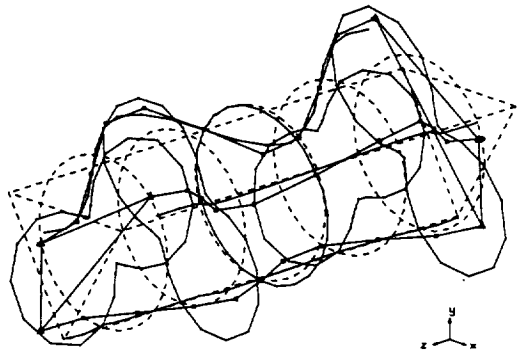

(d) i=2, j=4 Radial-Axial Mode (48.4 Hz)

Fig. 13 – Typical ATC Mode Shapes (Config. 1: Bare Frame)

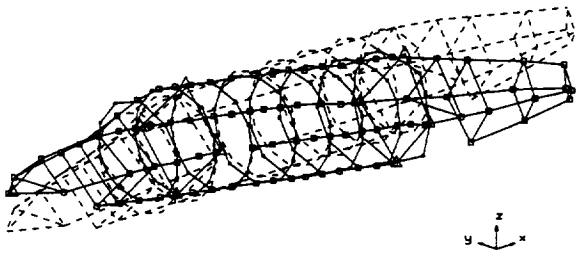

(a) Rigid-Body Pitch Mode (3.7 Hz)

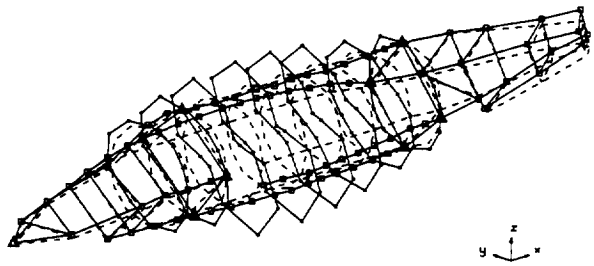

(b) i=2, j=1 Radial-Axial Mode (30.9 Hz)

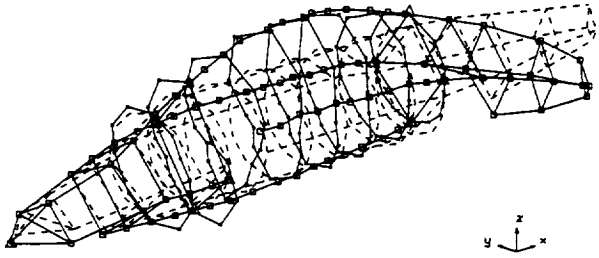

(c) 1st Vertical Bending Mode (36.4 Hz)

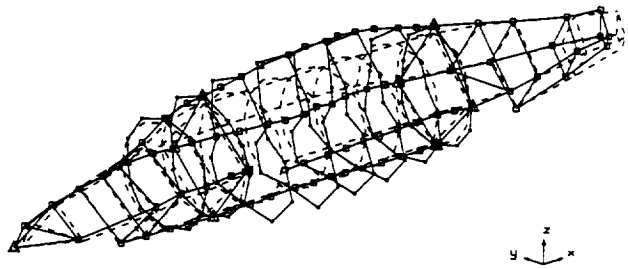

(d) i=3, j=1 Radial-Axial Mode (45.5 Hz)

Fig. 14 – Typical BSF Mode Shapes (Config. 1: Bare Fuselage Without Side Windows or Door)